4412 *Macromolecules* **2010**, *43*, 4412–4417
DOI: 10.1021/ma100162c

Macromolecules
ARTICLE

Constitutive Curve and Velocity Profile in Entangled Polymers during Start-Up of Steady Shear Flow

Keesha A. Hayes,[†] Mark R. Buckley,[‡] Haibo Qi,[†] Itai Cohen, and Lynden A. Archer*,[†]

[†]*School of Chemical & Biomolecular Engineering and* [‡]*Department of Physics, Cornell University, Ithaca, New York 14853*

Received January 28, 2010; Revised Manuscript Received March 8, 2010

ABSTRACT: Time-dependent shear stress versus shear rate, *constitutive curve*, and velocity profile measurements are reported in entangled polymer solutions during start-up of steady shear flow. By combining confocal microscopy and particle image velocimetry (PIV), we determine the time-dependent velocity profile in polybutadiene and polystyrene solutions seeded with fluorescent 150 nm silica and 7.5 μm melamine particles. By comparing these profiles with time-dependent constitutive curves obtained from experiment and theory, we explore the connection between transient nonmonotonic regions in the constitutive curve for an entangled polymer and its susceptibility to unstable flow by shear banding [Adams et al. *Phys. Rev. Lett.* **2009**, *102*, 067801-4]. Surprisingly, we find that even polymer systems which exhibit transient, nonmonotonic shear stress−shear rate relationships in bulk rheology experiments manifest time-dependent velocity profiles that are decidedly linear and show no evidence of unstable flow. We also report that interfacial slip plays an important role in the steady shear flow behavior of entangled polymers at shear rates above the reciprocal terminal relaxation time but has little, if any, effect on the shape of the velocity profile.

Introduction

Recent velocity profile measurements using micrometer-sized particles dispersed in entangled polybutadiene solutions show, for the first time, that steady shear flow of entangled polymer liquids is unstable to shear banding at moderate and high shear rates.[1−3] An important feature of these studies is that shear banding occurs even in moderately entangled polymer solutions, generally thought to be well-described by tube model constitutive theories amended to include mechanisms like convective constraint release[4−8] and Rouse relaxation of chain length.[9] Parameters such as shear strain and shear rate, widely used to characterize shear flow of entangled polymers, are ill-defined in a banded fluid. The presence of bands in these fluids therefore raises obvious questions about the reliability of decades worth of nonlinear rheological data obtained in these systems.

In a previous article,[10] we reported that confocal microscopy measurements can be used to recover the velocity profile in entangled polymers in a setting free of the secondary flow and edge effects that plague shear flow experiments of highly elastic polymers. Specifically, we used spatially resolved measurements of nanometer-sized, fluorescent tracers dispersed in entangled polymers undergoing shear flow in a narrow-gap ($H = 25-35$ μm), high-aspect ratio ($W/H > 142$), planar-Couette shear flow cell. We determined the velocity profile in polymer solutions covering a range of molecular weights and degrees of entanglement ($8 \leq Z \leq 56$). These experiments showed that the steady-state velocity profiles in all moderately entangled and some well-entangled polymer solutions are straight lines with slopes essentially equal to the applied shear rate, even at rates well into the non-Newtonian shear flow regime ($\dot{\gamma} \gg \tau_d^{-1}$). This finding is inconsistent with expectations for a shear-banded fluid.

For the remaining well-entangled polymer solutions, linear velocity profiles were also observed, but the slope values were found to diverge markedly from the imposed shear rate at rates smaller than $\dot{\gamma} \geq \tau_d^{-1}$, the onset of the non-Newtonian regime. In ref 10, this feature was analyzed by assuming that the solutions slip uniformly at the shear cell surfaces, and this analysis yielded slip velocity versus shear stress profiles, which were in agreement with earlier reports.[11] On this basis, it was concluded that when artifacts due to interfacial slip are avoided, the steady shear velocity profile in entangled polymer solutions is inconsistent with the notion that shear banding is a universal characteristic of these materials.

A perhaps obvious concern about this conclusion is that the phenomena analyzed as interfacial slip could well reflect the onset of bands, with the steepest bands localized within microscopic regions near both shear cell surfaces. This argument linking apparent slip violations in an entangled polymer to strong gradients in the velocity profile produced by nonmonotonic shear stresses in the bulk liquid is clearly not new.[12] It is also compatible with the recent particle velocimetry measurements in entangled polybutadiene solutions reported by Ravindranath and Wang,[13] in which interfacial slip sometimes preceded their observations of shear banding in polymers.

An arguably more intriguing explanation of earlier results comes from the recent theoretical studies of Adams and Olmsted,[14] which show that "shear-banding-like" behavior can be observed even for entangled polymers with a monotonic constitutive curve. Specifically, these authors used a version of Rolie−Poly (RP) model,[15] which was modified to include a stress "diffusion" term[16,17] to describe the fluid's response to an inhomogeneous viscoelastic stress. They solved the momentum conservation equation for entangled polymer liquids subject to steady shear flow in a variety of geometries. Results from this analysis reveal a phenomenon, we here term "apparent shear banding", which originates from spatial gradients in velocity and shear stress in curvilinear flow geometries. The phenomenon is expected to vanish at steady state in a planar-Couette shear

*To whom correspondence should be addressed.

 Published on Web 04/13/2010

Table 1. Properties of Entangled Polymer Solutions Used in This Study

sample	Z	τ_d (s)	$G_N \times 10^{-4}$ (Pa)	$\eta_0 \times 10^{-5}$ (Pa·s)
PBD200K, $\varphi = 0.6$ solvent: 5K PBD	56	0.92	46	2.7
PS8.42M, $\varphi = 0.06$ solvent: DEP	11	12.7	0.048	0.12

geometry but could result in pronounced transient shear bands in highly entangled polymer liquids when convective-constraint release and sub-Rouse, transient chain stretching effects are ignored.

In the current study, we extend our earlier confocal rheometry technique to characterize the velocity profiles in entangled polymers under *large-gap* conditions, designed to minimize interfacial slip effects.[18] Motivated by the recent analysis of Adams and Olmsted,[14] we also characterize the time-dependent evolution of the flow curve and velocity profiles in entangled polymer liquids during start-up of steady shear flow. An unexpected benefit of the former experiment is that the transient flow curve measurements provide unique insight into both the fluid-scale and molecular-scale response to a steady shear flow.

Experimental Section

Materials. Entangled polystyrene and polybutadiene solutions (Table 1) were used in all experiments reported. The polystyrene solution (PS8.42M6%, $Z \equiv N/N_e \approx 11$) was created by dissolving a high-molar-mass polystyrene melt, $\bar{M}_w = 8.42 \times 10^6$ g/mol, $\bar{M}_w/\bar{M}_n = 1.2$ (Tosoh Haas, Japan), in a mixture of diethyl phthalate (DEP) and tetrahydrofuran (THF, Sigma-Aldrich) as cosolvent. Entangled polybutadiene solutions (PBD200K60%, $Z = 56$) were likewise prepared by dissolving the corresponding high molar mass 1,4-polybutadiene melt, $\bar{M}_w = 2 \times 10^5$ g/mol, $\bar{M}_w/\bar{M}_n = 1.05$, (synthesized in-house), in a mixture of a weakly entangled PBD oligomer, $\bar{M}_w = 5 \times 10^3$ g/mol, and THF as cosolvent.

To characterize the velocity profile in these materials, they were seeded either with nanosized (diameter ~150 nm), fluorescent, core−shell, silica tracer particles, known as C dots [in narrow-gap studies], or with 7.5 μm spherical, melamine particles incorporating fluorescein isothiocyanate (FITC) (Corpuscular Inc.) [in large-gap studies]. C dots encapsulating a tetramethylrhodamine fluorophore in their core were synthesized using a variant of a previously published routine.[19−21] To maximize dispersion in the polymer solution, the C dots were first surface modified with *n*-hexadecyltrichlorosilane and dispersed in a tetrahydrofuran (THF) carrier solvent. The resultant polymer/solvent/THF solution was combined with the C dot/THF or dry melamine particles and mixed thoroughly using a magnetic stirrer. The THF cosolvent was subsequently evaporated at room temperature, and the last traces were driven off in a vacuum oven.

Apparatus. Details of the confocal rheology measurement device (Figure 1) and procedure used to recover the velocity profile have been reported previously.[10] In the current study, the time-dependent velocity profiles in polymer solutions with average number of entanglements per chain, Z, of 11 and 56 were characterized using narrow gap ($H \approx 75\,\mu$m) and large-gap ($H \approx 230-425\,\mu$m), planar-Couette shear flow measurements. A perhaps obvious disadvantage of the large-gap experiments is that the sample aspect ratio is large, which makes the measurements, particularly at high shear rates $\dot{\gamma} \geq \tau_d^{-1}$, susceptible to artifacts produced by secondary flow.[22] To reduce this effect, the area A_s of the top (stationary/measuring) plate was increased from 5 mm^2 (narrow-gap experiments) to 7 mm^2 (large-gap experiments), yielding aspect ratios ($a_s = W/H$) ≥ 14. In addition to the obvious advantage of reducing the influence of wall slip on the velocity profile, the larger gaps allow for concomitantly

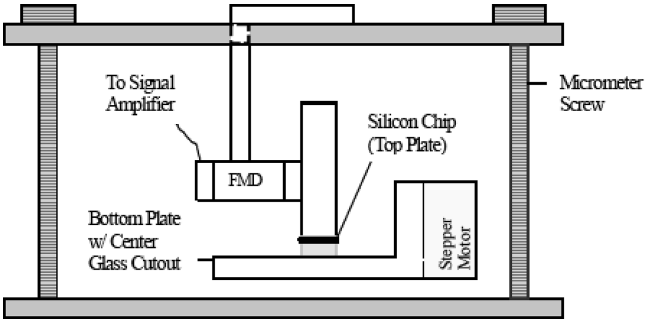

Figure 1. Schematic (front view) of planar-Couette shear cell used for the confocal experiments.

larger tracers, which allows measurements to be performed at lower magnification (10×). The feature is advantageous because it allows tracers to be measured in a wider field of view, which provides a more effective method for interrogating possible secondary flows in the solutions. To ascertain that all the particle sizes used function exclusively as tracers, small-amplitude oscillatory shear measurements were performed in all samples with and without particles and verified to be unaffected by the particles.

To characterize the velocity profile during shear flow, software adapted from MATPIV was used to measure the instantaneous particle speed in different layers throughout the planar-Couette cell gap.[23] A force measurement device (FMD),[10] attached to the top shearing surface, was used to simultaneously measure the shear force during start-up of steady shear. The FMD is connected to a signal conditioning amplifier, and before sample loading, the FMD was calibrated. Different loads are applied to the top plate and the corresponding change in voltage (ΔV) is recorded. $\sigma = F/A_s$, and in the resulting calibration curve, $F = k(\Delta V)$, where k = constant. The maximum response/compliance time, $\tau^T \leq \eta_0 A_s K/H$, for the device can be computed at any gap H, provided the material's zero shear viscosity η_0 and the compliance of the instrument K are known. Using standard beam deformation equations,[24] we determine that the instrument compliance $K \approx 10\ \mu$m/N, which is about 3 times the nominal value for the torsional compliance for the force rebalance transducer (FRT) in the Rheometrics Scientific Ares rheometer. Substituting zero shear viscosities from Table 1, we therefore conclude that for $H = 75\ \mu$m $\tau^T_{PS8.42M6\%} \leq 8$ ms and $\tau^T_{PBD200K60\%} \leq 180$ ms; the corresponding compliance times at the largest gap, $H = 425\ \mu$m, studied are $\tau^T_{PS8.42M6\%} \leq 2$ ms and $\tau^T_{PBD200K60\%} \leq 45$ ms.

By synchronizing the time intervals at which the velocity profile was recorded with the transient shear force measurement times, it was possible to interrogate the profile in the full range of stress regimes (i.e., from start-up, $t = 0$, to steady state, $t = t_{ss}$ (defined here as the time required for the shear force to reach a plateau; see Figure 2). Anticipating a comparison with the mechanism proposed by Adams and Olmsted,[14] we recognize that there are two equally plausible methods for projecting information obtained from transient flow curve data to understand the velocity profiles obtained from PIV experiments. Specifically, because the measurements are performed in as ideal a planar-Couette shear flow geometry as experimentally possible, absent a transition to a shear banded state, the shear rate in the gap $\dot{\gamma}$ is a constant at essentially all observation times. This means that although our velocity profile measurements are performed at a fixed observation time, t_m, they can be thought of as being performed at a fixed applied shear strain, $\gamma_a = \dot{\gamma} t_m$.

As a complement to the planar-Couette shear measurements, time-dependent shear stress measurements were conducted during start-up of steady shear flow at a wide range of shear rates. These measurements were performed using a Rheometric Scientific (ARES) rheometer outfitted with cone and plate

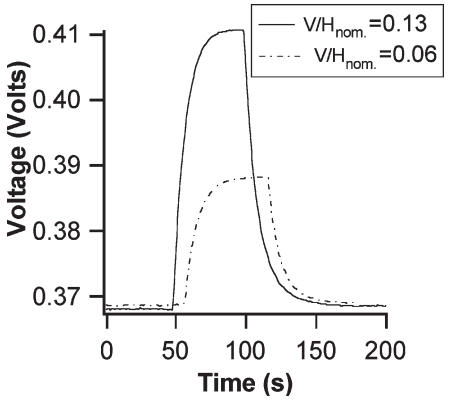

Figure 2. Typical FMD response obtained from confocal rheology experiments during start-up of steady shear flow for PS8.42M6% with $H = 75\ \mu$m.

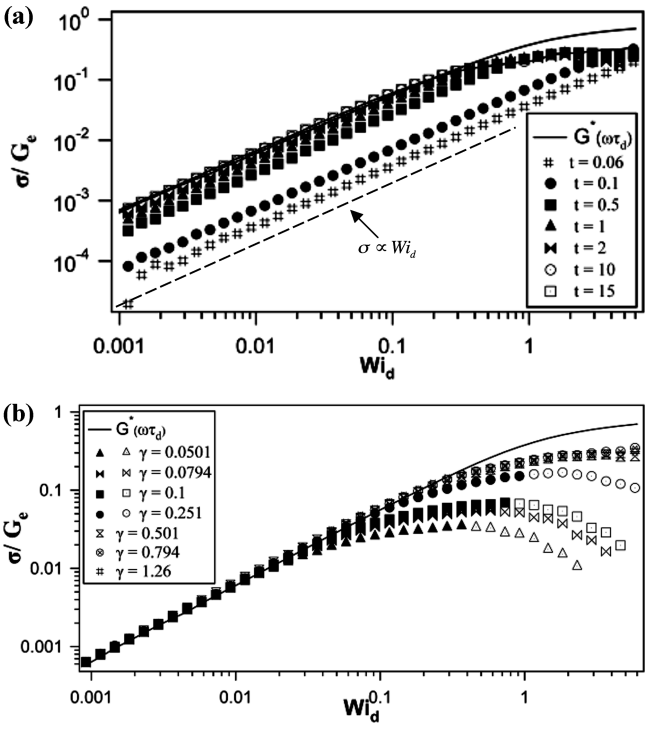

Figure 3. Dimensionless constitutive curves for PBD200K60%_5K: (a) at various observation times, in seconds; (b) at various shear strains.

fixtures: CP10mm-5.4° and CP25mm-5°. An important benefit is that by plotting the measured shear stresses at fixed observation time, t_m, or for specific values of the imposed shear strain, γ_a, constitutive curves, $\sigma(\dot{\gamma})$ vs $\dot{\gamma}$, can be facilely determined as a function of t_m or γ_a under similar flow conditions and, for the same materials, investigated in planar-Couette shear flow.

Results and Discussion

Figure 3a reports the instantaneous constitutive curves σ/G_e versus $Wi_d \equiv \dot{\gamma}\tau_d$ for PBD200K60%. The plateau modulus G_e used to nondimensionalize the shear stress was obtained from oscillatory shear measurements in the linear viscoelastic (LVE) regime, from which G_e is determined as the storage modulus value that corresponds to the loss minimum in the plateau regime. The characteristic relaxation time, τ_d, was also determined from LVE experiments as the reciprocal of the oscillatory shear frequency, ω, at which the imaginary part of the complex viscosity, $\eta''(\omega) \equiv G'(\omega)/\omega$, manifests a global maximum, i.e., just prior to the terminal regime. The solid line in Figure 3a is the constitutive

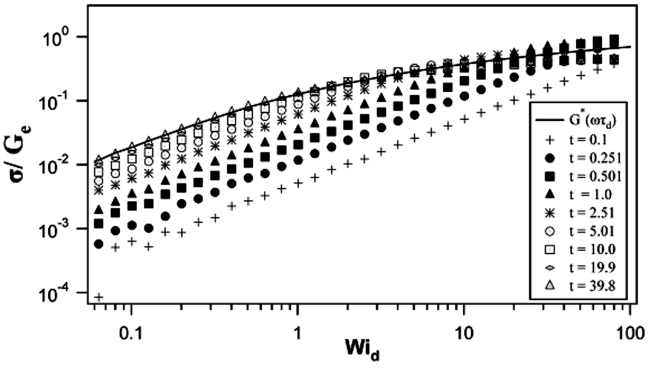

Figure 4. Dimensionless constitutive curves for PS8.42M6% as a function of observation time in seconds.

curve, $\sigma(Wi_d) = G^*(\omega\tau_d)$, obtained by enforcing the Cox−Merz rule, which states that the steady-state shear viscosity, $\eta(\dot{\gamma}) \equiv \sigma(\dot{\gamma})/\dot{\gamma}$, measured in a continuous shear flow is equal to the complex viscosity $\eta^*(\omega) \equiv G^*(\omega)/\omega$ measured in small-amplitude oscillatory shear flow.

Figure 3a shows that at the earliest observation times the shear stress increases monotonically, in reality linearly (broken line), with dimensionless shear rate, Wi_d, over the entire range of rates studied. For transient shear stress data at a fixed observation time t_m, this observation is equivalent to saying that the shear stress is proportional to the applied shear strain $\gamma_a = \dot{\gamma}t_m$, implying that the material's initial response is purely elastic and that microscopic material elements deform affinely in response to the macroscopic deformation. At longer observation times, the shear stress continues its monotonic increase with rate up to an observation-time-dependent dimensionless shear rate (Wi_d), at which the shear stress becomes independent of both the shear rate and applied shear strain. In particular, at an observation time of 0.5 s, the monotonic response regime ends at a critical dimensionless shear rate $Wi_{d,c} \approx 1$, whereas for an observation time of 15 s ($t_m/\tau_d \approx 17$), it ends at $Wi_{d,c} \approx 0.4$.

For $Wi_d > Wi_{d,c}$, the shear stress shows little, if any, dependence on observation time, regardless of the shear rate. The continuous line in the figure is the constitutive curve obtained from steady state oscillatory shear measurements in the linear viscoelastic regime. Comparison of this line with the steady shear data (symbols) indicates that the Cox−Merz rule does not hold for $Wi_d > Wi_{d,c}$, i.e., over the same range where the shear stress becomes approximately independent of rate. Taken together, these observations imply that the steady state (long-time) flow curves at moderate-to-high shear rates present the only scenario where this polymer might be unstable to shear banding.

Figure 3b shows constitutive curves for the same polymer measured at various discrete shear strains. The figure shows that at the smallest applied strains ($\gamma_a \leq 0.25$) the flow curve is not a monotonic function of rate, and there is a maximum in $\sigma(\dot{\gamma})$. The open symbols on these curves ($\gamma_a \leq 0.25$) are stress data, $\sigma(t)$, corresponding to times below the torsion compliance time $\tau_T = 5\pi\eta_0 D^3/6\alpha K_T$ of the force-rebalance transducer (FRT) and, as such, are untrustworthy.[25] If these points are ignored, one reaches a similar conclusion as for the constitutive curves at constant observation time, namely that the flow is most unstable to banding at a critical dimensionless shear rate $Wi_{d,c} \approx 0.1$. However, in this case the unstable regime extends over the largest shear rate range at the smallest observation strains.

Figure 4 shows that the conclusions reached above are not unique to polybutadiene solutions or to highly entangled or highly concentrated polymer liquids. Specifically, this figure plots the constitutive curves for a ultrahigh molecular weight polystyrene in diethyl phthalate (see Table 1). Although its solution

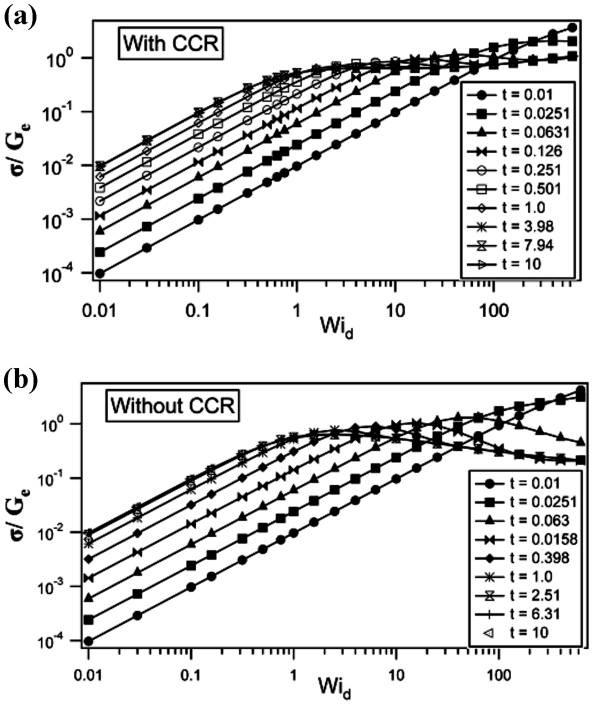

Figure 5. Dimensionless constitutive curves predicted by the IA constitutive equation as a function of observation time: (a) with CCR; (b) without CCR.

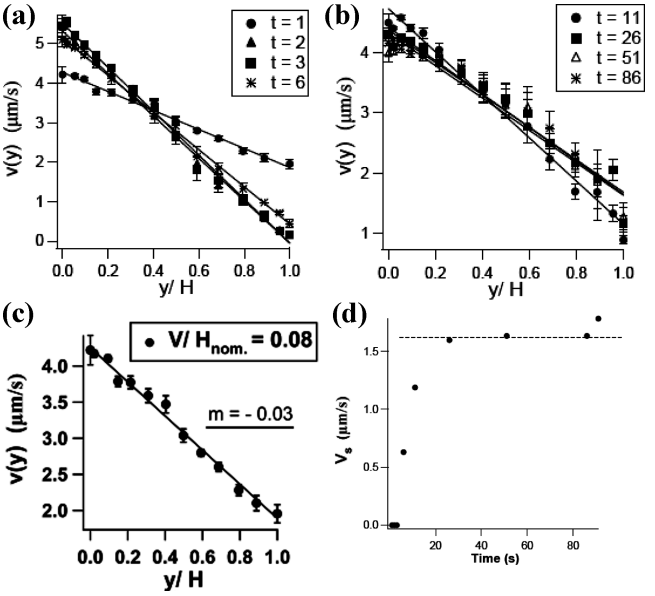

Figure 6. Time-dependent velocity profiles for PS8.42M 6% at $H = 75\,\mu$m and $\dot{\gamma}_{nom} = (V/H)_{nom} = 0.08\ s^{-1}$: (a) early time profiles; (b) long-time behavior; (c) steady state; (d) apparent slip velocity versus time. All times are in seconds.

volume fraction is lower, this polymer has a much longer terminal time, $\tau_d = 12.7$ s, which makes the unstable constitutive regime accessible at lower shear rates.

To rule out well-known mechanical artifacts (e.g., edge fracture and slip at the wall[26]) as the source of the observations in Figures 3 and 4, we used a version of the differential constitutive model proposed by Islam and Archer[27] to predict the constitutive curves for an entangled polymer with entanglement density ($Z=20$), intermediate between the two materials studied experimentally. An advantage of this analysis is that we can systematically turn on/off different molecular scale physics to evaluate their role in the observed behaviors. Figure 5a,b reports the calculated dimensionless stress versus dimensionless shear rate for this polymer when the convective constraint release (CCR) relaxation mechanism[4] is present/absent. Because CCR provides a mechanism for the shear flow to accelerate polymer chain relaxation, relative to reptation diffusion, its absence in the model is expected to produce higher levels of chain orientation at all shear rates $\dot{\gamma} \geq \tau_d^{-1}$. Recent flow dielectric relaxation studies by Watanabe and co-workers[28] raise new doubts about the role of CCR in entangled polymer relaxation dynamics; studying the model with CCR suppressed is therefore not merely an academic exercise.

Figure 5b shows that if relaxation via CCR is not included in the analysis, decidedly nonmonotonic constitutive curves are observed on time scales before the onset of reptation and persist even at steady state. Conversely, the polymer appears to recover from this intermediate, unstable state if CCR is included in the analysis. Both figures therefore show behaviors qualitatively similar to what is observed experimentally—for both materials. Figure 5a, in particular, provides a near-identical replication of the time-dependent evolution of the constitutive curve seen experimentally. Significantly, it shows that even with CCR present the material manifests a nonmonotonic constitutive curve and is therefore unstable toward banding. Additionally, Figure 5a indicates that the regime of greatest vulnerability to shear banding is largest at the longest observation times (steady state) and extends to dimensionless shear rates below unity. The first of these features is evidently inconsistent with arguments advanced in the Introduction to support transient banding. It in fact implies that the velocity profile at steady state provides the most plausible/realistic scenario for observing shear band formation in entangled polymers.

Next, we determine what role, if any, these bulk constitutive behaviors play in the evolution of the velocity profile in entangled polymers subject to simple shear flow. To this end, we carried out transient PIV experiments in the planar-Couette shear geometry at shear rates covering a similar range as in the shear rheology measurements. Figure 6 summarizes results for PS8.42 M at a gap $H = 75\ \mu$m and an imposed shear rate $\dot{\gamma} = 0.08\ s^{-1}$, which corresponds to $Wi_d = \dot{\gamma}\tau_d \approx 1$. It is apparent from the figure that, with the exception of an initial induction period of about 1 s (Figure 6a), the velocity profile changes little with time at short times and is essentially linear at all times. While it is tempting to attribute this short-time behavior to instrument compliance, the time scales are at least 2 orders of magnitude too large (i.e., compared to $\tau^T_{PS8.42M6\%}$.

The only evidence of possible nonlinearities come from the long-time profiles, wherein particles nearest to either plane appear to move marginally slower than the expected speeds obtained by extrapolating the straight line fits of the data to these locations in the shear cell. At long times, a trend toward lower slopes (actual/true shear rates) is observed (Figure 6b). The velocity near the stationary plane of the planar-Couette shear cell is larger (nonzero) than expected, and the velocity near the moving plane becomes progressively smaller. Figure 6c compares the slope m of the steady state, long-time, velocity profile with the nominal (imposed shear rate). It is apparent from the figure that the actual shear rate experienced by the fluid in the gap is substantially smaller than the imposed shear rate. All of the features seen in Figure 6 are consistent with the existence of measurable levels of interfacial slip in the material and a substantial diminution of the imposed shear.

The degree to which the fluid is observed to slip at a particular time is easily calculated from the measured, $\dot{\gamma}_T = m$, and imposed/nominal, $\dot{\gamma}_{nom} = (V/H)_{applied}$, shear rates. If the slip is taken to occur equally at the stationary and moving planes of the cell, the instantaneous slip velocity at any given time can be computed

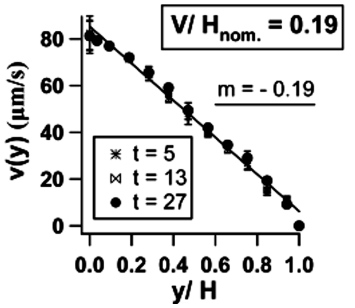

Figure 7. Time-dependent velocity profiles for PS8.42M6% at H = 425 μm and $\dot{\gamma}_{nom} = (V/H)_{nom} = 0.19\ s^{-1}$. All times are in seconds.

using the formula $V_s = (H/2)(\dot{\gamma}_{nom} - \dot{\gamma}_T)$. Slip velocities determined in this way are plotted in Figure 6d, which clearly shows that the level of slip increases with time and reaches a steady state at a time close to twice the terminal time for the polymer. These observations are consistent with our previous report[10] and imply that slip—not bands—is the more likely manifestation of the susceptibility to unstable flow deduced from the experimental and theoretical constitutive curves. That the slip velocity in an entangled polymer follows similar time-dependent dynamics as the shear stress is also consistent with earlier works on slip.[18,29,30]

An unsatisfying feature of the results in Figure 6 is that slip prevents sufficiently high shear rates to be achieved in the material to access the high Wi_d flow regime where the constitutive curve reveals greatest vulnerability to instability by shear banding. For a fixed slip velocity, the difference between the nominal and true shear rate in a polymer undergoing shear flow in a planar-Couette geometry should vary as the inverse of the plane separation. This means that measurements at larger cell gaps could be advantageous. Figure 7 is the time-dependent velocity profile obtained for PS8.42M6% at a gap about 5 times larger than that used for the results in Figures 6. A limitation of our measuring technique at these larger gaps is that only moderate shear rates can be achieved. The results in Figure 7 are for a nominal shear rate of 0.19 s^{-1}, which is for all practical purposes identical to the actual shear rate in the material, m. The corresponding dimensionless shear rate $Wi_d \approx 2.5$, which places the material in the most unstable regime in the constitutive curve. Figure 7, nonetheless, shows decidedly linear velocity profiles, which manifest no detectable dependence on time. This finding simultaneously confirms our earlier point that time-dependent slip is the source of the transient changes in the velocity profiles in Figure 6 and that, contrary to expectations from the time-dependent constitutive curves, the material is stable with respect to shear band formation.

Figure 8 summarizes the corresponding velocity profiles for the more highly entangled polymer solution, PBD200K60%. These measurements were also performed at a large shear cell gap ($H \approx 225\ \mu$m) to minimize interfacial slip. The velocity profile is again seen to initially vary substantially with time for the first 2 s or so following start-up, but then to become time-independent. Comparing these time scales to $\tau^T_{PBD200K60\%} \leq 60$ ms, we again conclude that the short-time profile is unlikely to originate from instrument compliance.

At all times, including the ~2 s start-up/induction period, the profiles are again seen to be linear, with the slope at steady state (Figure 8b) identical to what is expected for the applied speed. On the basis of the constant-observation time constitutive curves for this material (Figure 3a), the dimensionless shear rate for the largest shear velocity (highest rate, $\dot{\gamma}_T \approx 0.4\ s^{-1}$) that can be reliably achieved in our experiment are close to Wi_{dc}; it is substantially higher for the constant-strain case (Figure 3b). At rates beyond this value, macroscopic voids/fissures are observed

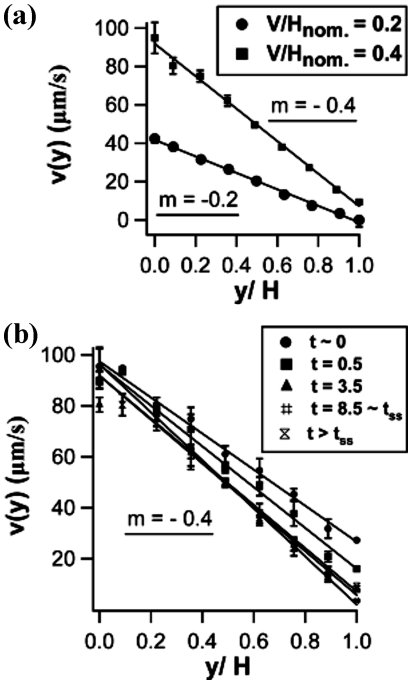

Figure 8. Velocity profiles for PBD200K60%_5K at H = 223 μm: (a) steady state profiles at $\dot{\gamma}_{nom}$ = 0.2 and 0.4 s^{-1}; (b) time-dependent profiles for $\dot{\gamma}_{nom} = 0.4\ s^{-1}$.

to spring up at the interface between the polymer and shear fixtures, beginning at the edges, and quickly engulfing the interface, rendering velocity profile measurements with our experimental technique meaningless at shear rates above those in Figures 7 and 8. In particular, in this surface-void-dominated regime, pockets of fluid near the interface occasionally appear to move at velocities different from that extrapolated from bulk, but at other locations the profiles appear linear throughout the material. Although this behavior might be interpreted as evidence of banding, the clear, visible influence of voids makes this characterization incongruent with what one normally means by a constitutive instability. Work underway in the group focuses on applying surface treatments to the planar-Couette cell fixtures, which have been reported previously to delay void formation[11] and to suppress interfacial slip,[18] to extend the range of Weissenberg numbers at which transient velocity profiles in entangled polymers can be recovered with our measurement technique.

Conclusions

We have used time-resolved rheological data during start-up of steady shear flow to characterize the time evolution of the *constitutive curve* $\sigma(\dot{\gamma})$ vs $\dot{\gamma}$ in entangled polymer solutions. Constitutive curves constructed at fixed observation times exhibit a nonmonotonic regime for moderate and highly entangled solutions at long times (steady state) and high dimensionless shear rates, $Wi_d > 1$. Constitutive curves constructed at constant shear strains manifest multivalued regimes at all strains, with the effect being most apparent at low and moderate values of the shear strain, where the regime begins at $Wi_d < 0.1$. Using a differential constitutive model for the stress, we show that these observations are of microscopic origin and are exacerbated when convective acceleration of polymer relaxation (CCR) by reptation diffusion is ignored.

Taken together, our observations imply that a zone of instability should exist in entangled polymer liquids where phenomena such as shear banding and flow reversal might be observed. To evaluate this conclusion, we use a confocal rheology technique (confocal microscopy and PIV) to create time-dependent maps of

the velocity profiles in the same fluids during start-up of steady shear flow in a planar-Couette geometry. These measurements reveal no evidence of unstable flow but show substantial evidence of time-dependent interfacial slippage in the polymers. By performing planar-Couette shear flow measurements at larger cell gaps, we show that slip effects can be eliminated, allowing the polymer response to its constitutive curve to be studied at moderately higher Wi_d. As with the experiments performed at smaller gaps, however, these measurements reveal decidedly linear velocity profiles at all times, with no evidence of unstable or shear/banded flow. At higher shear rates, large deformable voids become visible at the fluid/solid interface, beginning at the three phase (air/fluid/solid) contact line, which limits the range of shear rates at which velocity profile measurements are possible.

While our findings do not rule out transient bands in start-up of steady shear flow of entangled polymers at shear rates above those achieved with our planar-Couette shear flow device, they do mean that the requirements for entangled polymers to exhibit even transient shear banding in this geometry are more complex than one might infer from literature reports in other geometries. Additionally, our finding that interfacial slip and interfacial voids dominate both the transient and steady-state fast flow behaviors of entangled polymer liquids at small and large gaps implies that under continuous shear flow these fluids are more likely to exhibit discontinuities in velocity at or near the fluid/solid interface than in bulk.

Acknowledgment. This work was supported by Award No. KUSC1-018-02, made by King Abdullah University of Science and Technology (KAUST) and by the National Science Foundation (Award No. CBET-0756516). We are grateful to Erik Herz and Prof. Ulrich Wiesner for providing the surface-functionalized fluorescent nanoparticle tracers used in the study.

References and Notes

(1) Tapadia, P.; Wang, S. Q. *Phys. Rev. Lett.* **2006**, *96*, 016001–4.
(2) Tapadia, P.; Ravindranath, S.; Wang, S. Q. *Phys. Rev. Lett.* **2006**, *96*, 196001–4.
(3) Boukany, P. E.; Wang, S. Q. *J. Rheol.* **2007**, *51*, 217–233.
(4) (a) Ianniruberto, G.; Marrucci, G. *J. Rheol.* **2001**, *45*, 1305–1318. (b) *J. Non-Newtonian Fluid Mech.* **2002**, *102*, 383−395.
(5) Milner, S. T.; McLeish, T. C. B.; Likhtman, A. E. *J. Rheol.* **2001**, *45*, 539–563.
(6) Graham, R. S.; Likhtman, A. E.; Mead, D. W.; Larson, R. G.; Doi, M. *Macromolecules* **1998**, *31*, 7895–7914.
(7) Bent, J.; et al. *Science* **2003**, *301*, 1691–1695.
(8) Graham, R. S.; Likhtman, A. E.; McLeish, T. C. B. *J. Rheol.* **2003**, *47*, 1171–1200.
(9) (a) McLeish, T. C. B.; Ball, R. C. *J. Polym. Sci., Polym. Phys. Ed.* **1986**, *24*, 1735–1745. (b) McLeish, T. C. B. *J. Polym. Sci., Polym. Phys. Ed.* **1987**, *25*, 2253–2264.
(10) Hayes, K. A.; Buckley, M. R.; Cohen, I.; Archer, L. A. *Phys. Rev. Lett.* **2008**, *101*, 218301–4.
(11) Mhetar, V. R.; Archer, L. A. *Macromolecules* **1998**, *31*, 6639−6649, 8607−8616.
(12) Cates, M. E.; McLeish, T. C. B.; Marrucci, G. *Europhys. Lett.* **1993**, *21*, 451–456.
(13) Ravindranath, S.; Wang, S. Q. *J. Rheol.* **2008**, *52*, 957–980.
(14) Adams, J. M.; Olmsted, P. *Phys. Rev. Lett.* **2009**, *102*, 067801–4.
(15) Likhtman, A. E.; Graham, R. S. *J. Non-Newtonian Fluid Mech.* **2003**, *114*, 1–12.
(16) Olmsted, P. D.; Radulescu, O.; Lu, C. Y. D. *J. Rheol.* **2000**, *44*, 257–275.
(17) Adams, J. M.; Fielding, S. M.; Olmsted, P. D. *J. Non-Newtonian Fluid Mech.* **2008**, *151*, 101–118.
(18) Sanchez-Reyes, J.; Archer, L. A. *Langmuir* **2003**, *19*, 3304–3312.
(19) Ow, H.; Larson, D. R.; et al. *Nano Lett.* **2005**, *5*, 113–117.
(20) Burns, A.; Ow, H.; Wiesner, U. *Chem. Soc. Rev.* **2006**, *35*, 1028–1042.
(21) Herz, E.; Burns, A.; et al. *Proc. SPIE* **2006**, *6096*, 1–12.
(22) Mhetar, V. R.; Archer, L. A. *J. Rheol.* **1996**, *40*, 549–571.
(23) Keane, R. D.; Adrian, R. J. *Appl. Sci. Res.* **1992**, *49*, 191–215.
(24) Ashby, M.; Jones, D. *Engineering Materials: An Introduction to Their Properties and Applications*; Pergamon Press: Oxford, 1980.
(25) Dutcher, C. S.; Venerus, D. C. *J. Non-Newtonian Fluid Mech.* **2008**, *150*, 154–161.
(26) Inn, Y. W.; Wissbrun, K. F.; Denn, M. M. *Macromolecules* **2005**, *38*, 9385–9388.
(27) Islam, M. T.; Archer, L. A. *J. Polym. Sci., Part B* **2001**, *39*, 2275–2289.
(28) Uneyama, T.; Masuubuchi, Y.; Horio, K.; Matsumiya, Y.; Watanabe, H.; Pathak, J. A.; Roland, C. M. *J. Polym. Sci., Part B* **2009**, *47*, 1039–1057.
(29) Archer, L. A.; Chen, Y.-L.; Larson, R. G. *J. Rheol.* **1995**, *39*, 519–525.
(30) (a) Dao, T. T.; Archer, L. A. *Langmuir* **2002**, *18*, 2616–2624. (b) Mhetar, V. R.; Archer, L. A. *Macromolecules* **1998**, *31*, 8607–8616.